Dynamics of gas–solid interactions: Calculations of energy transfer and sticking

Mary Shugard and John C. Tully

Bell Laboratories, Murray Hill, New Jersey 07974

Abraham Nitzan

Department of Chemistry, Tel Aviv University, Tel Aviv, Israel
and Bell Laboratories, Murray Hill, New Jersey 07974
(Received 15 November 1976)

A classical mechanical generalized Langevin formalism is applied to the study of gas–surface collisions. Procedures are described for constructing generalized friction and fluctuating forces which accurately represent the motion of real solids, and which can be conveniently implemented in a classical stochastic trajectory calculation. Energy transfer computed using this approach for He–W collisions is in excellent agreement with results of a quantum mechanical distorted wave calculation employing the same phonon density of states. The method is further applied to the study of residence times and sticking probabilities. Results indicate that the stochastic trajectory approach is feasible and capable of accurate simulation of gas–surface collision phenomena.

I. INTRODUCTION

A major problem in gas–surface collision theory is incorporation of lattice many-body effects, i.e., treatment of energy exchange between gas molecules and the solid. Several approaches to this problem have been proposed, ranging from simple "cube" models[1] to full scale numerical solution of the equations of motion of a sizeable cluster of atoms.[2] Previous classical and quantum mechanical studies of this type are summarized in a review by Goodman and Wachman.[3]

Recent developments by Adelman and Doll (hereafter referred to as AD) represent an important advance in this area.[4,5] They combine the generalized Langevin equation (GLE) formalism of Kubo[6] and Mori[7] with standard classical mechanical (gas-phase) scattering techniques. Their formulation, in principle, encompasses the effects of an infinite lattice at nonzero temperature to arbitrarily high accuracy.

The basic idea of the approach is as follows: atoms are classified into three groups, gas atoms (R), a small number of primary lattice atoms (P), and the remaining secondary lattice atoms (Q). The formulation rests on two basic assumptions. First, interactions between gas atoms and the solid depend on the instantaneous positions of the primary lattice atoms, but not on the instantaneous positions of secondary lattice atoms. Second, interactions among the secondary lattice atoms and between the secondary and primary lattice atoms are harmonic. Under these assumptions, we can write the following matrix equations governing the motions of the three types of atoms:

$$\ddot{\mathbf{x}}_R(t) = \mathbf{M}_{RR}^{-1}\,\mathbf{F}_R[\mathbf{x}_R(t)\ ,\ \mathbf{x}_P(t)]\ , \tag{1}$$

$$\ddot{\mathbf{x}}_P(t) = -\,\mathbf{M}_{PP}^{-1/2}\,\Omega_{PP}^2\,\mathbf{M}_{PP}^{1/2}\,\mathbf{x}_P(t) - \mathbf{M}_{PP}^{-1/2}\,\Omega_{PQ}^2\,\mathbf{M}_{QQ}^{1/2}\,\mathbf{x}_Q(t) + \mathbf{M}_{PP}^{-1}\,\mathbf{F}_P[\mathbf{x}_R(t),\ \mathbf{x}_P(t)]\ , \tag{2}$$

$$\ddot{\mathbf{x}}_Q(t) = -\,\mathbf{M}_{QQ}^{-1/2}\,\Omega_{QP}^2\,\mathbf{M}_{PP}^{1/2}\,\mathbf{x}_P(t) - \mathbf{M}_{QQ}^{-1/2}\,\Omega_{QQ}^2\,\mathbf{M}_{QQ}^{1/2}\,\mathbf{x}_Q(t)\ . \tag{3}$$

The forces $\mathbf{F}_R$ and $\mathbf{F}_P$ describing the interactions between the gas and the lattice are completely arbitrary. Ω_{PP}^2 is the matrix describing the harmonic interactions among the primary atoms P; Ω_{QQ}^2 is the corresponding matrix for the secondary atoms Q; and $\Omega_{QP}^2 = \Omega_{PQ}^{2\dagger}$ describes the harmonic coupling between P and Q atoms. $\mathbf{M}_{RR}$, $\mathbf{M}_{PP}$, and $\mathbf{M}_{QQ}$ are the matrices of masses of gas, primary lattice, and secondary lattice atoms, respectively.

Equation (3) can be solved formally and substituted into Eq. (2), giving after some manipulation

$$\ddot{\mathbf{x}}_P(t) = -\,\Omega_{eff}^2\,\mathbf{x}_P(t) - \Lambda(t)\,\mathbf{x}_P(0) - \int_0^t \Lambda(t-t')\,\dot{\mathbf{x}}_P(t')\,dt' + \mathbf{M}_{PP}^{-1}\,\mathbf{R}(t) + \mathbf{M}_{PP}^{-1}\,\mathbf{F}_P[\mathbf{x}_R(t)\ ,\ \mathbf{x}_P(t)]\ , \tag{4}$$

where

$$\Omega_{eff}^2 = \mathbf{M}_{PP}^{-1/2}\,[\Omega_{PP}^2 - \Lambda(0)]\,\mathbf{M}_{PP}^{1/2}\ , \tag{5}$$

$$\Lambda(t) = \mathbf{M}_{PP}^{-1/2}\,\Omega_{PQ}^2\cos(\Omega_{QQ}\,t)\,\Omega_{QQ}^{-2}\,\Omega_{QP}^2\,\mathbf{M}_{PP}^{1/2}\ , \tag{6}$$

and

$$\mathbf{R}(t) = -\,\mathbf{M}_{PP}^{1/2}\,\Omega_{PQ}^2\cos(\Omega_{QQ}t)\,\mathbf{M}_{QQ}^{1/2}\,\mathbf{x}_Q(0) - \mathbf{M}_{PP}^{1/2}\,\Omega_{PQ}^2\sin(\Omega_{QQ}t)\,\Omega_{QQ}^{-1}\,\mathbf{M}_{QQ}^{1/2}\,\dot{\mathbf{x}}_Q(0)\ . \tag{7}$$

Equations (4)–(7) are exact, and are equivalent to those derived by AD.[5]

Thus, we have replaced the infinite set of coupled equations (1)–(3) with a small number of equations (1) and (4). The matrix Ω_{eff}^2 appearing in the GLE, Eq. (4), is an effective frequency matrix. As discussed by AD,[5] $\mathbf{R}(t)$ can be considered a Gaussian random force, with a frequency spectrum that is characteristic of the lattice. The damping (friction) kernel $\Lambda(t)$ is related to $\mathbf{R}(t)$ through the second fluctuation–dissipation theorem.[5,6] This follows directly from Eqs. (6) and (7),

$$\langle \mathbf{R}(0)\,\mathbf{R}^\dagger(t)\rangle = k_B T\,\mathbf{M}_{PP}\,\Lambda(t)\ , \tag{8}$$

where brackets denote ensemble average, k_B is the Boltzmann constant, T is temperature, and we have made use of the relations

$$\langle \mathbf{x}_Q(0)\,\mathbf{x}_Q^\dagger(0)\rangle = k_B T\,\mathbf{M}_{QQ}^{-1/2}\,\Omega_{QQ}^{-2}\,\mathbf{M}_{QQ}^{-1/2}\ , \tag{9}$$

and

$$\langle \mathbf{x}_Q(0)\,\dot{\mathbf{x}}_Q^\dagger(0)\rangle = 0\ , \tag{10}$$

which are valid for a harmonic lattice in thermal equilibrium.

Adelman, Doll, and Myers[4,5,8,9] show that by linearizing the stochastic differential equation (1) and (4), equations of a Fokker–Planck form for the particle probability distribution functions can be generated. They demonstrate convincingly that in cases where linearization is valid, this procedure is far more efficient than direct solution of Eqs. (1) and (4).[8] Unfortunately, linearization is justified only when particle trajectories do not deviate excessively from the zero-noise trajectory. Therefore, this procedure cannot be expected to be useful except perhaps for the simplest direct atom–surface encounters. The method does not appear capable of describing such processes as trapping, molecular dissociation, desorption, or chemical reaction.

In this paper we investigate the feasibility of obtaining direct numerical solutions of the GLE's, Eqs. (1) and (4), via Monte Carlo sampling of classical stochastic trajectories. Related studies by Adelman and Garrison[10] and by Doll and Dion[11] have just been reported. In the next section we discuss the implementation of this procedure. We focus particularly on the question of how to employ known lattice properties to construct the generalized friction kernel $\Lambda(t)$, fluctuating force $R(t)$, and effective frequency Ω_{eff}^2 required in the GLE, Eq. (4). We describe a simple procedure for producing a fluctuating force and generalized friction that is capable of accurately representing the properties of real lattices. We apply this method, in Sec. III, to calculate energy exchange during a collinear atom–surface collision at a variety of surface and gas temperatures. Results are compared to those obtained by the quantum mechanical single phonon approach of Lennard-Jones, Devonshire, and Strachan.[12] In Sec. IV we apply the method to trapping collisions, thereby demonstrating its utility for such problems and shedding further light on the role played by the damping and fluctuating forces. The final section is a short appraisal of the outlook of the generalized Langevin formalism for describing the dynamics of realistic gas–surface interactions.

II. STOCHASTIC TRAJECTORIES

The GLE's, Eqs. (1) and (4), can be solved numerically for the classical stochastic trajectories which describe the motion of the gas and primary surface atoms. This can be carried out by a procedure analogous to the familiar classical trajectory method employed for gas-phase collisions.[13] The classical trajectory method requires prior specification of the forces of interaction between the atoms for all relevant interatomic separations, i.e., of a potential energy hypersurface. This has been done to varying degrees of accuracy by methods ranging from *ab initio* quantum chemical calculations to empirical fitting of experimental data. Analogously, the generalized Langevin approach described here requires specification of the forces of interaction among the gas atoms and between the gas and primary surface atoms. In the calculations reported in this paper we employ simple model potentials and do not address the question of constructing accurate interactions for realistic systems.

In addition to the interatomic forces F_R and F_P of Eqs. (1) and (4), the generalized Langevin approach requires specification of the effective frequencies Ω_{eff}^2, damping kernels $\Lambda(t)$, and fluctuating forces $R(t)$ defined in Eqs. (5)–(7). The success of the approach depends on how effectively these quantities can be designed to mimic the motion of the solid. Methods for obtaining these quantities from known properties of the solid, and implementing them into the numerical procedure for generating stochastic trajectories, are the subject of this section. Questions concerning the accuracy and utility of the approach are addressed in succeeding sections.

Our object is to find connections between measurable properties of the solid and the microscopic quantities in the GLE which are to represent the infinite number of degrees of freedom which are not explicitly treated. To show how this can be done, consider a case where the primary lattice consists of a single atom, and where all gas atoms are distant so the interaction F_P vanishes in the GLE, Eq. (4). By multiplying Eq. (4) on the lhs by $\dot{x}_P(t=0)$ and performing an ensemble average over initial conditions and initial values of $R(t)$, we obtain

$$\frac{d}{dt}\langle \dot{x}_P(0)\,\dot{x}_P(t)\rangle = -\Omega_{eff}^2\langle \dot{x}_P(0)\,x_P(t)\rangle - \int_0^t \Lambda(t-t')\langle \dot{x}_P(0)\,\dot{x}_P(t')\rangle\,dt' \quad , \tag{11}$$

where we have made use of the relations

$$\langle \dot{x}_P(0)\,x_P(0)\rangle = 0 \quad , \tag{12}$$

and

$$\langle \dot{x}_P(0)\,R(t)\rangle = 0 \quad . \tag{13}$$

Equation (13) follows directly from the definition of the fluctuating force, Eq. (7).

Taking the cosine transform of Eq. (11), we obtain

$$C_{vv} = \frac{2}{\pi}\int_0^\infty dt\cos(\omega t)\langle \dot{x}_P(0)\,\dot{x}_P(t)\rangle = \frac{(2/\pi)\omega^2\Lambda_c(\omega)\langle \dot{x}_P(0)\,\dot{x}_P(0)\rangle}{[\omega^2-\Omega_{eff}^2-\omega\Lambda_s(\omega)]^2+\omega^2\Lambda_c^2(\omega)} \quad , \tag{14}$$

where C_{vv} is the cosine transform of the velocity autocorrelation function, and $\Lambda_c(\omega)$ and $\Lambda_s(\omega)$ are $\pi/2$ times the cosine and sine transforms of the damping kernel of Eq. (6):

$$\Lambda_c(\omega) = \int_0^\infty dt\cos(\omega t)\,\Lambda(t) \quad , \tag{15}$$

$$\Lambda_s(\omega) = \int_0^\infty dt\sin(\omega t)\,\Lambda(t) \quad . \tag{16}$$

Equation (14) is an exact relation between the velocity autocorrelation function, an observable, and the quantities Ω_{eff}^2 and $\Lambda(t)$ appearing in the GLE. For atoms in translationally invariant systems for which the x, y, and z directions are equivalent, e.g., a bulk atom in a 3D simple cubic lattice, the normalized cosine transform of the velocity autocorrelation function is equal to the phonon density of states $g(\omega)$.[14] Thus we have

$$g(\omega) = \frac{2}{\pi} \frac{\omega^2 \Lambda_c(\omega)}{[\omega^2 - \Omega_{eff}^2 - \omega \Lambda_s(\omega)]^2 + \omega^2 \Lambda_c^2(\omega)} \quad . \tag{17}$$

More general relations are required for more complicated lattice structures.

Equations (14) and (17) allow us in principle to determine Ω_{eff}^2 and $\Lambda(t)$ from presumably known information about the solid. To accomplish this we propose a specific functional form for $\Lambda(t)$, to be described below, and then choose the parameters in this function to best reproduce the behavior of the surface. This also provides us with the autocorrelation function of the fluctuating force, $\langle R(0)R(t)\rangle$, through the fluctuation-dissipation theorem, Eq. (8).

The simplest possible choice for $\Lambda(t)$ would be

$$\Lambda(t) = \beta\delta(t) \ , \tag{18}$$

where β is a constant and $\delta(t)$ is the delta function. We will refer to this as the *Brownian limit*. In this limit the damping no longer retains memory of previous times, and the fluctuating force $R(t)$ becomes white noise; i.e., Eq. (4) becomes identical to the phenomenological Langevin equation. Figure 1 illustrates the cosine transform of the velocity autocorrelation function, C_{vv} of Eq. (14), and $\Lambda_c(\omega)$ of Eq. (15) obtained by the approach using typical values of β and Ω_{eff}, the only two parameters. We would expect the Brownian limit to be useful when the time scale of the thermal motion of the solid is fast compared to the motion of the colliding gas particles. Since this is rarely the case for realistic gas–solid collision phenomena, we must view this approximation with suspicion. The validity of the Brownian limit is examined computationally in Sec. IV.

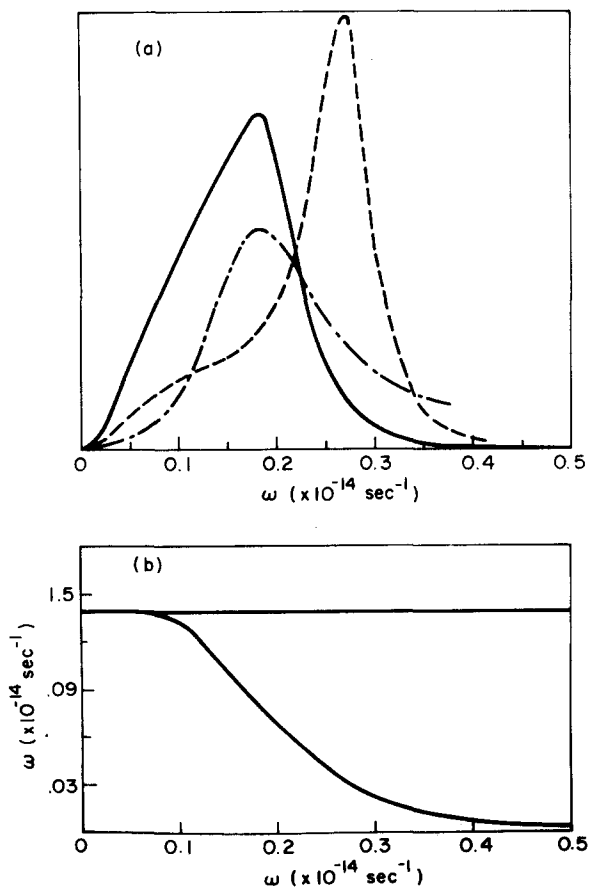

FIG. 1. (a) The density of states for a bulk solid (dashed) curve), and the surface density of states generated from it using Eq. (20) (solid curve). The dash–dot curve is the density of states for a Brownian oscillator. (b) The cosine transform of the friction kernel associated with the surface oscillator (smooth curve), and the Brownian oscillator (straight line).

A more realistic functional form for $\Lambda(t)$ is the following:

$$\Lambda(t) = \Lambda_0 e^{-(1/2)\gamma t}[\cos(\omega_1 t) + \tfrac{1}{2}\gamma\omega_1^{-1}\sin(\omega_1 t)] \ . \tag{19}$$

This is the form of the position autocorrelation function of a Brownian oscillator.[15,16] It exhibits the damped oscillatory behavior expected for lattice atoms. As shown in Fig. 1(b), $\Lambda_c(\omega) \to 0$ as $\omega \to \infty$, in contrast to the Brownian limit. This can have important consequences with respect to accommodation of high frequency motion, as discussed in Sec. IV.

As illustrated in Fig. 1(a), Eq. (19) can reproduce the qualitative shapes of typical density of states spectra. More complicated spectra can be constructed using a linear combination of two or more terms of the form of Eq. (19). The justification for using Eq. (19), in addition to physical arguments, is ease of computation. Generation of the damping functional and fluctuating force produced by Eq. (19) can be accomplished easily and exactly by the procedure outlined in the Appendix.

In order to apply this approach to a realistic situation, we need to choose values of four parameters Λ_0, γ, and ω_1 of Eq. (19) and Ω_{eff}^2. In some cases we may have direct information about the velocity autocorrelation function of surface atoms, e.g., from electron diffraction experiments or from molecular dynamics simulations. In such cases we can use Eq. (14) directly, selecting parameters to best fit C_{vv}. In other cases we may not have enough information about surface dynamics but do know the bulk phonon density of states, e.g., from neutron diffraction. It may then be possible to use the bulk data to obtain satisfactory estimates of the four parameters appropriate for the surface.

As an illustration, consider the perpendicular (z-direction) motion of a surface atom in a 3D simple cubic lattice. We can use the bulk density of states in Eq. (17) to choose the parameters Λ_0, γ, ω_1, and Ω_{eff}^2 to optimally describe the z-direction motion of a bulk atom. A typical example of $g(\omega)$ generated in this way is given by the dashed line in Fig. 1(a). The main contribution to $\Lambda(t)$ is due to the two nearest neighbors of the bulk atom in the $\pm z$ direction. A surface atom differs from a bulk atom, very crudely speaking, in that one of these two neighbors is missing. It is not unreasonable to estimate that the frequency and decay parameters ω_1 and γ of the damping kernel remain unchanged while the strength parameter Λ_0 and squared oscillator frequency Ω_{eff}^2 are reduced by roughly a factor of 2 for a surface atom compared to the bulk. The solid curve in Fig. 1(a) is the resulting cosine transform of the velocity autocorrelation function for motion of a surface atom in the perpendicular direction, obtained from the bulk density of

states shown by the dashed curve of Fig. 1(a), using the following relations:

$$\Lambda_0(\text{surface}) = \tfrac{1}{2}\Lambda_0(\text{bulk}) ,$$

$$\gamma(\text{surface}) = \gamma(\text{bulk}) ,$$

$$\omega_1(\text{surface}) = \omega_1(\text{bulk}) ,$$

$$\Omega_{\text{eff}}^2(\text{surface}) = \tfrac{1}{2}\Omega_{\text{eff}}^2(\text{bulk}) . \quad (20)$$

This is an example of a very crude way in which bulk information can be used to provide surface parameters. In cases where information about force constants is known, a procedure that is similar in spirit to this but systematic and accurate can be formulated.

In this section we have attempted to show how quantities appearing in the GLE, Eq. (4), might be obtained from information about the solid. Once the effective frequencies Ω_{eff}, friction kernels $\Lambda(t)$, and interaction forces F_R and F_P have been specified, numerical solution of the GLE's proceeds almost exactly as in a gas-phase classical trajectory study. Initial conditions (vibrational phases, vibrational amplitudes, impact parameters, etc.) are selected at random from distributions chosen to mimic the experimental situation to be simulated.[13] The only additional complication incurred with the generalized Langevin approach is initialization of the fluctuating force and damping terms in Eq. (4), both of which have memory of previous times. While this may pose some problems in certain situations, e.g., surface diffusion or desorption studies, for gas–surface collision simulations of the type reported here, the problem is easily eliminated. All that is required is to begin the calculation with gas–surface separation sufficiently large that the damping and fluctuating force terms have time to randomize before impact.

Once initial conditions have been selected, a stochastic trajectory is generated by numerical integration of Eqs. (1) and (4), including the fluctuating force and generalized friction terms, which can be easily treated by the method described in the Appendix. In the applications discussed below we have employed an Adams–Moulton predictor–corrector numerical integrator, with Runge–Kutta–Gill starter.[13] Once the trajectory is completed, a new set of initial conditions (and a new sequence of the random force) are selected and a new trajectory computed. This process is repeated until adequate statistics on the outcome of the collision are generated.

III. ENERGY TRANSFER AND ACCOMMODATION

Here we apply the method described in the previous section to the calculation of energy transfer during an atom solid collision. Energy transfer, usually expressed in terms of energy and thermal accommodation coefficients, has long been a popular observable in the study of nonreactive interactions between gases and solid surfaces. The subject has been recently extensively reviewed.[3] Our main concern here is not merely to provide an additional method for calculating accommodation coefficients, but mainly to demonstrate on a simple, familiar system that the method of classical stochastic trajectories provides a simple, reliable, and relatively cheap way to perform computations on nonreactive lattice gas interactions.

With this objective in mind we have performed computations on a one-dimensional model for the collision of a helium atom with tungsten solid surface. Only one primary lattice atom was considered. A purely repulsive interaction $\exp(-br)$ was assumed, where r is the distance between the He atom and the primary surface W atoms, and b is taken to be 1.3 Å^{-1}.[3] The parameters describing the lattice have been chosen to yield the best fit to a Debye spectrum with Debye temperature 380 °K (W bulk Debye temperature). The corresponding surface parameters have then been obtained as described in Sec. II. The bulk parameters are $\Omega_{\text{eff}} = 2.488\times10^{13}$ sec^{-1}, $\Lambda_0 = 1.238\times10^{27}$ sec^{-2}, $\gamma = 4.975\times10^{13}$ sec^{-1}, and $\omega_1 = 2.488\times10^{13}$ sec^{-1}; while for the corresponding surface parameters we have $\Omega_{\text{eff}} = 1.759\times10^{13}$ sec^{-1} and $\Lambda_0 = 6.19\times10^{26}$ sec^{-2}. The bulk and surface density of state functions which correspond to these parameters are displayed in Fig. 2.

To test the reliability of the classical stochastic trajectory approach we have compared the results obtained by this method to those obtained using the quantum mechanical Lennard-Jones, Devonshire, and Strachan (LJDS) approach.[12] We have used the single phonon approximation in the form

$$P(\omega) = \frac{8\pi^2 M_g^2 |\omega|}{b^2 M_s \hbar} g(|\omega|) F(\omega) \frac{\sinh(\pi q_I)\sinh(\pi q_F)}{[\cosh(\pi q_I) - \cosh(\pi q_F)]^2} ,$$

$$q_I = \frac{2}{b\hbar}\sqrt{2M_g E_g} ,$$

$$q_F = \frac{2}{b\hbar}\sqrt{2M_g(E_g - \hbar\omega)} ,$$

$$F(\omega) = \begin{cases} n(\omega)+1 & \omega > 0 \\ n(\omega) & \omega < 0 \end{cases} , \quad (21)$$

where M_g and M_s are the masses of the gas and solid atoms, $g(\omega)$ is the density of surface phonons, $n(\omega) = [\exp(\hbar\omega/kT) - 1]^{-1}$ is the thermal population function, and E_g is the gas atom initial kinetic energy. $P(\omega)$ represents the probability density that the gas atom gives to ($\omega > 0$) or takes from ($\omega < 0$) the solid an amount $\hbar\omega$ of energy during the collision process. For the small mass ratio of the He–W system and for incident energies which are not too large (such that multiphonon pro-

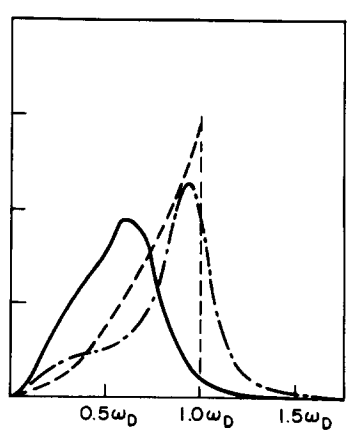

FIG. 2. The Debye spectrum of a solid (dashed curve). The bulk density of states chosen to fit this Debye spectrum (dash–dot curve), and the surface density of states derived from it using Eq. (20).

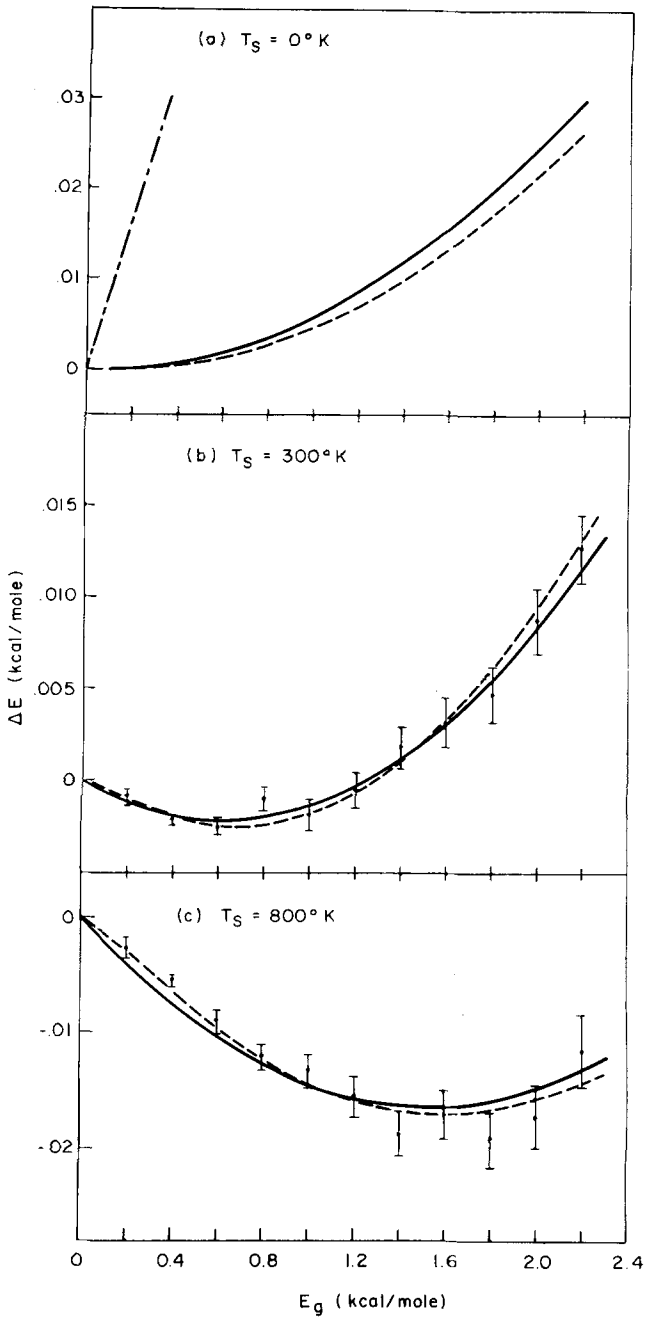

FIG. 3. The results of a calculation of energy transfer for various incident gas beam energies. The dashed curves were obtained from the quantum mechanical calculation. The points with error bars are the results of the classical calculation. The solid curves are the results of a least squares fit to these points. The dash-dot curve in (a) is the hard-sphere limit.

cesses are unimportant), the LJDS approach, which is based on the Jackson–Mott distorted wave approximation,[17] is expected to yield results which are accurate to within a few percent. In what follows we compare these results to those obtained using the classical stochastic trajectories approach. We use exactly the same surface density of states in both calculations. We compute the energy transfer as well as the second moment of the distribution $P(\omega)$, both for a well-defined initial energy E_i of the incident atom and for a Maxwell–Boltzmann distribution corresponding to a given gas temperature.

In Figs. 3(a)–3(c) we present the result of the calculation of the average energy transfer to the solid as a function of the incident atom energy for three different surface temperatures. The classical trajectory results have been obtained (for surface temperatures $T_s > 0$) by averaging over 10^4 trajectories. For any surface temperature except zero the average energy transfer has a minimum. This is of course expected as collisions are adiabatic at $E_g = 0$; at small incident energy $\langle \Delta E \rangle$ is less than zero (for T_s greater than zero), reflecting the fact that the gas atom gains energy during the collision process while as E_g becomes larger $\langle \Delta E \rangle$ has to change its sign. The minimum in $\langle \Delta E \rangle$ occurs at incident energy for which E/k is roughly equal to the surface temperature, which implies the existence of a region with negative energy accommodation coefficients. In all cases the agreement between the classical and the quantum mechanical results is remarkably good.

The thermally averaged energy transfer resulting from the classical and quantum mechanical calculations for gas temperature $T_g = 300$ °K is displayed in Fig. 4. The quantum mechanical results are obtained by averaging Eq. (21) over a Maxwell–Boltzmann distribution for E_g. The classical average has been done using a least square fit of the results of Fig. 3(b) to a second-order polynomial. Thermal accommodation coefficients are presented in Table I.

In addition, we have tested the behavior of the classical trajectories for very high incident energies and verified the approach to the hard sphere result:

$$\Delta E = -\frac{4\mu}{(1+\mu)^2} E_g , \quad T_s = 0 . \tag{22}$$

The close agreement between the classical and the quantum results should not be taken as evidence for the suitability of the classical approach for any calculation

TABLE I. Thermal accomodation coefficients.[a]

T_g \ T_s	0 °K	300° K	800° K
100° K	2.78 (1.40)	1.72 ± 0.37 (2.00)	2.14 ± 0.17 (2.02)
200° K	4.79 (3.62)	3.83 ± 1.01 (4.54)	4.76 ± 0.28 (4.59)
300° K	7.25 (5.98)		7.26 ± 0.33 (7.17)
400° K	9.71 (8.31)	8.04 ± 1.22 (9.57)	9.49 ± 0.50 (9.65)
500° K	12.2 (10.6)	10.6 ± 1.2 (11.9)	11.4 ± 1.3 (11.9)
600° K	14.3 (12.7)	12.9 ± 1.4 (14.1)	12.3 ± 3.3 (14.2)
700° K	14.5 (14.8)	14.2 ± 4.9 (16.2)	9.3 ± 10.5 (16.3)

[a]The values listed are in units of 10^{-3}. The classical calculation values are given first. The values obtained from the quantum calculation are given in parentheses.

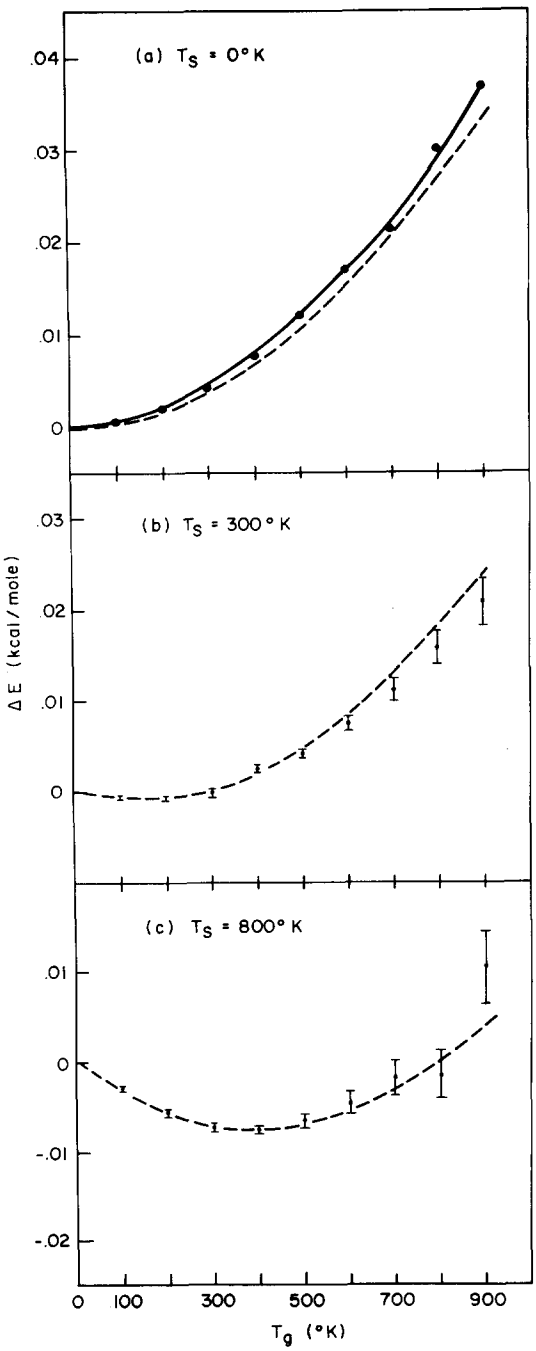

FIG. 4. Energy transfer for various thermal beam gas temperatures. The points and solid curves are the results of the classical calculations. The dashed curves are the results of the quantum calculations.

of this kind. This depends mainly on the nature of the observable. To show this we give in Table II the E_g dependence of the second moment of the distribution $P(\omega)$. Here the results differ at low temperatures, reflecting the fact that the zero temperature classical trajectory is unique while in the quantum case there is a finite spread of ΔE.

It is interesting to note that the energy transfer ΔE as associated with a collision of the incident atom with a single harmonic oscillator is very unreliable as an estimate for the true $\langle \Delta E \rangle$. The reason is that, depending on the choice of parameters, ΔE may be strongly dependent on the oscillator frequency. This is the case for the He–W system where ΔE changes by 3 orders of magnitude over the spectrum of the solid.

In conclusion, the stochastic trajectory approach has been shown to be an accurate and practical way for performing computations on direct (nonsticking) gas–surface collisions. In the next section we extend the method to the study of adsorption and desorption processes.

IV. TRAPPING AND RESIDENCE TIMES

In this section, we apply the stochastic classical trajectory approach to the calculation of sticking probabilities and residence times in gas–solid collisions. Our primary concerns here are to demonstrate that the method is flexible enough to treat these problems and to investigate the dependence of the method on the forms of the stochastic elements used. We apply the method to a one-dimensional model for the collision of gas atoms of various masses with a solid composed of atoms of mass 184.

The interaction is taken to be a Morse potential with a shallow well:

$$V(r) = \{D_0[1 - e^{-\alpha r}]^2 - D_0\} \ , \tag{23}$$

where r is the distance between the gas atom and the single primary surface atom. For the purposes of this study the potential parameters were chosen to be $D_0 = 0.75$ kcal/mole, and $\alpha = 1.2$ a.u.$^{-1}$. To model the solid, we again employ a generalized friction kernel of the form of Eq. (19), with parameters given by $\Lambda_0 = 2.01\times10^{26}$ sec^{-2}, $\gamma = 2.83\times10^{13}$ sec^{-1}, and $\omega_1 = 1.417\times10^{13}$ sec^{-1}. The effective frequency Ω_{eff} of Eq. (4) was taken to be 1.0×10^{13} sec^{-1}. The resulting surface density of states is given by the solid curve in Fig. 1(a). It can be thought of as arising from the bulk density of states given by the dashed curve in Fig. 1(a), using the prescription of Eq. (20). Because of our unrealistic assumption of collinear collisions, we have made no attempt here to reproduce the true tungsten phonon density of states. Nevertheless, the density of states we employ is a fairly reaonsable one, and it would be possible using one or two terms of the form of Eq. (19) to

TABLE II. Widths of energy transfer distributions.

T_s	E_g(kcal/mole)	$\langle(\Delta E)^2 - \langle\Delta E\rangle^2\rangle$ (kcal/mole)^2	
		Classical	*Quantum*
300°K	0.19872	1.83×10^{-4}	2.00×10^{-4}
	0.39743	9.17×10^{-4}	9.23×10^{-4}
	0.59615	2.29×10^{-3}	2.25×10^{-3}
	0.79487	4.24×10^{-3}	4.21×10^{-3}
	0.99359	6.93×10^{-3}	6.84×10^{-3}
	1.1923	1.02×10^{-2}	1.01×10^{-2}
	1.3910	1.33×10^{-2}	1.40×10^{-2}
	1.5897	1.85×10^{-2}	1.85×10^{-2}
	1.7885	2.34×10^{-2}	2.37×10^{-2}
	1.9872	2.87×10^{-2}	2.92×10^{-2}
0°K	0.19872	0.00	5.34×10^{-6}
	1.9872	0.00	4.39×10^{-3}

obtain a quite accurate reproduction.

Calculations based on the generalized Langevin equation with these parameters are referred to as Case I. In addition we have carried out calculations in the Brownian approximation (see Sec. II) in order to investigate the necessity of using a friction kernel with memory and a non-white-noise random force.[18] The Brownian parameters were generated from the Case I parameters in the following way:

Case II: The effective frequency is chosen to be the same as in Case I, and the friction constant is taken to be the time integral of the damping kernel defined by Eq. (19). The numerical values obtained for this case are

$$\Omega_{eff} = 1.0\times10^{13}\ \text{sec}^{-1}\ ,$$

$$\beta = \int_0^\infty \Lambda(t')\,dt' = 0.709\times10^{13}\ \text{sec}^{-1}\ .$$

Case II is the classical definition of the Brownian limit.

Case III: We choose Ω_{eff} to match the peak position and β to be equal to the half-width at half-height of $\rho^{(\omega)}_{\text{surface}}$. Their values are

$$\Omega_{eff} = 1.842\times10^{13}\ \text{sec}^{-1}\ ,$$

$$\beta = 0.1417\times10^{14}\ \text{sec}^{-1}\ .$$

These values match very closely values which would be obtained using Adelman and Doll's prescription for the Brownian parameters

$$\Omega_{eff} = \omega_D/\sqrt{3}\ ,$$

$$\beta = \pi\omega_D/6\ ,$$

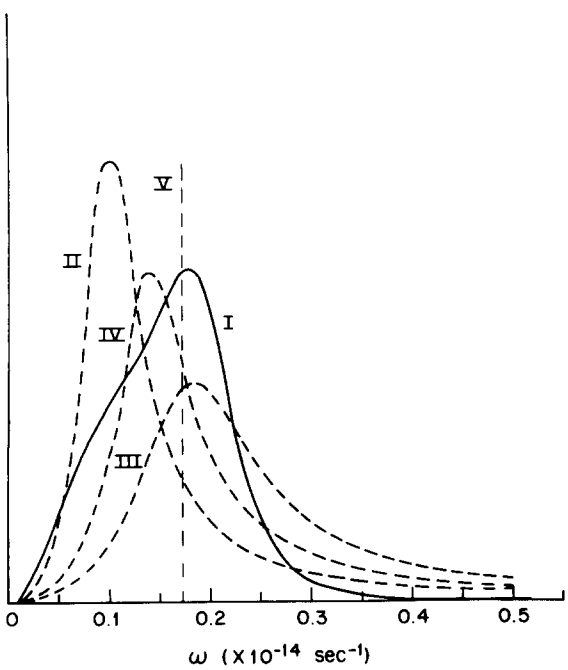

FIG. 5. The density of states for a generalized Langevin oscillator (Case I), for various Brownian oscillators (Cases II–IV), and for a single bare harmonic oscillator (Case V).

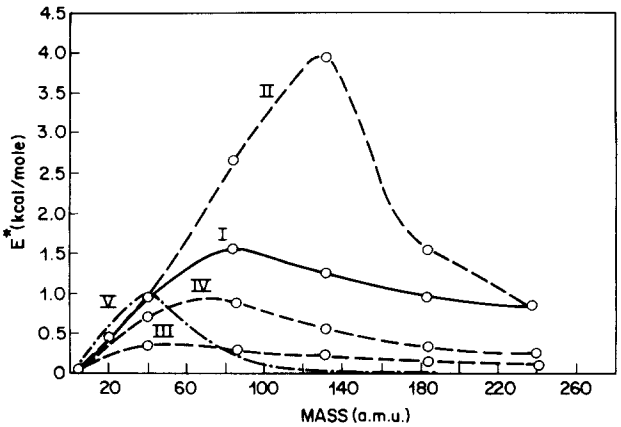

FIG. 6. The critical trapping energy for various incident gas masses for Cases I–V as defined in text.

with a value of ω_D which is consistent with our bulk density of states.

Case IV: We choose Ω_{eff} and β such that the frequency spectrum of the Brownian oscillator matches as closely as possible $\rho^{(\omega)}_{\text{surface}}$. This leads to

$$\Omega_{eff} = 1.417\times10^{13}\ \text{sec}^{-1}\ ,$$

$$\beta = 0.0945\times10^{14}\ \text{sec}^{-1}\ .$$

The frequency spectra of these Brownian oscillators are pictured in Fig. 5.

In addition to the Brownian approximation, we investigate the case of a single harmonic oscillator with no damping. We choose the frequency of the undamped oscillator to be the unshifted frequency of the generalized Langevin oscillator Ω_{pp} of Eq. (5). This gives us a fifth case.

Case V:

$$\Omega_{pp} = \sqrt{\Omega_{eff}^2 + \Lambda_0} = 1.735\times10^{13}\ \text{sec}^{-1}\ .$$

To test the difference between the generalized Langevin approach, the Brownian approximation, and the bare oscillator, we have undertaken an extensive study of the sticking probability for atoms of varying masses with a surface at 0 °K. For these 0 °K model calculations there exists a critical incident gas energy above which nothing will trap and below which everything traps. The sticking probability is given directly in terms of this critical energy E^*. For a monoenergetic beam

$$P_{\text{sticking}} = \begin{cases} 1 & E < E^* \\ 0 & E > E^* \end{cases}\ . \tag{24}$$

For a thermal beam of temperature T,

$$P_{\text{sticking}} = (1 - e^{-E^*/k_BT})\ . \tag{25}$$

We have measured this critical trapping energy for gas particle masses of 4, 20, 40, 84, 131, 184, and 238 colliding with a solid composed of atoms of mass 184 and modeled according to each of the five cases discussed above. The results are plotted in Fig. 6. The curves all have the same general shape. At first the sticking probability increases with increasing mass as the energy transfer becomes larger. At still higher

masses, the atom loses so much energy upon the initial collision that it stays in the interaction long enough for the solid atom to help push it out, so the sticking probability goes down again. Comparing the generalized Langevin results with the zero friction results, we see that for masses below 40, the effect of damping is to lower the sticking probability. The friction kernel, which might be pictured as a viscous medium surrounding the oscillator, has a response time which is long compared to the collision time so the particle is inefficient at transferring energy to it. The major effect of friction is to make the oscillator stiffer and thereby reduce sticking. As the mass increases, the collision time gets longer and the atom can efficiently transfer energy, so the effect of friction is to increase the sticking probability. In the case of the Brownian oscillator, the friction enters as a constant which is independent of time; hence it does not respond properly to changes in the collision time. We see the shapes of the curves of E^* vs mass for most of the Brownian cases are completely different from that of the generalized Langevin behavior. For Case IV, where we choose the spectrum of the Brownian oscillator to approximately match the surface density of states, the general shape is correct, but in the region where the damping begins to help increase sticking, we see the critical energy differs by as much as a factor of 2.

These studies indicate that results obtained from modeling a solid in the Brownian limit are very sensitive to the choice of the Brownian parameters used. They also imply that it is not possible to find a single choice of Brownian parameters which can reproduce at every mass the results of a solid modeled with a generalized friction force.

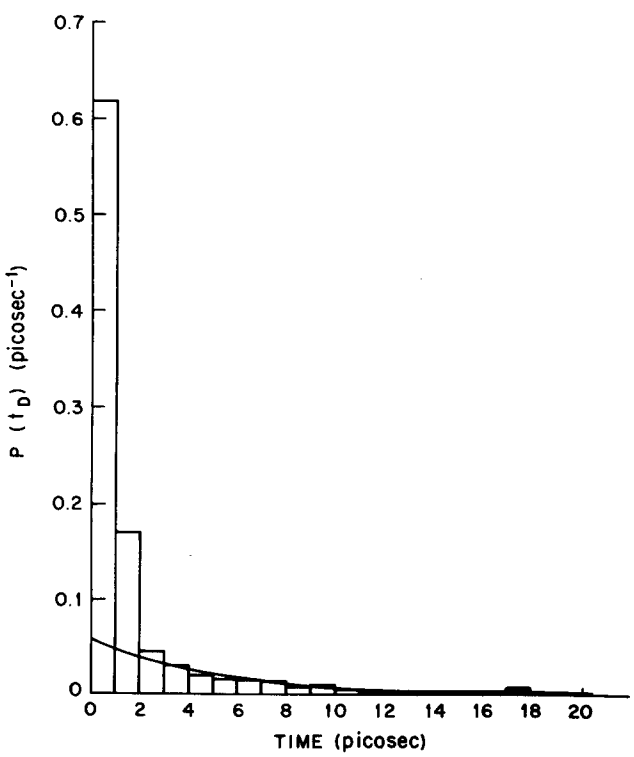

FIG. 7. Histogram plot of $P(t_D)$ obtained from stochastic trajectories for incident energy of 2.4 kcal/mole and $T_s = 300$ °K. The smooth curve is an exponential fit of the long time tail.

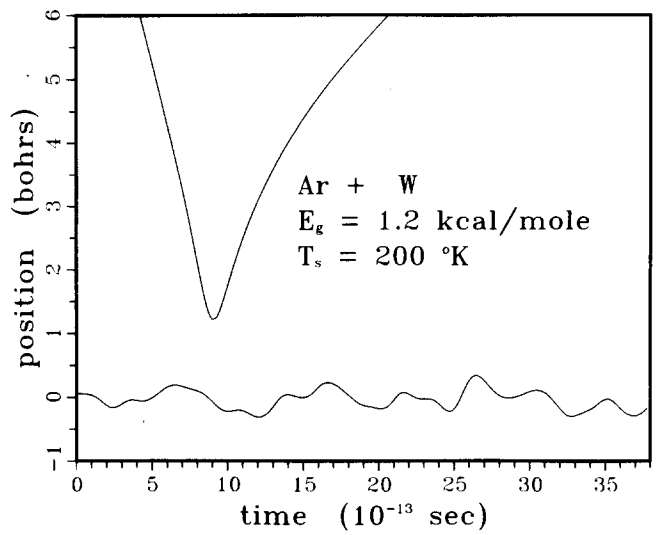

FIG. 8. Typical direct trajectory, showing the positions of the primary surface and gas atoms as a function of time.

The 0 °K results presented above probe effects of the friction kernel but not the fluctuationg force. To study the effects of using a correlated random force rather than one with a white noise spectrum, we have performed calculations at nonzero temperature. At nonzero temperature, concepts such as sticking probability and mean residence time do not have unique definitions. We define them so that they can be obtained from a single function $P(t_D)$, the time delay function. Consider a hypothetical experiment in which an ensemble of gas atoms is prepared at position r_0 outside the range of interaction of the surface and directed toward the surface with velocity v_0. The time delay function is defined such that $P(t_D)dt_D$ is the fraction of particles which, in traveling to the surface and back to position r_0, experience a time delay between t_D and $t_D + dt_D$. The time delay t_D is defined to be

$$t_D = t - t_0 \ , \tag{26}$$

where t_0 is the shortest time required for any of the particles in the ensemble to return to r_0. Defined in this way, $P(t_D)$ is independent of any assumptions about the spatial extent of the surface region. We take $P(t_D)$ to be normalized:

$$\int_{-\infty}^{\infty} P(t_D)\, dt_D = 1 \ . \tag{27}$$

A typical histogram plot of $P(t_D)$ is shown in Fig. 7. The function is composed of two parts, a sharp peak at small t_D arising from direct trajectories, and an exponentially decaying tail due to atoms which have been trapped and collide with the surface several times before desorbing. Typical examples of each type of trajectory are shown in Figs. 8 and 9.

We define a lifetime, τ, of trapped species from the exponential tail of $P(t_D)$ by fitting it to a function of the form $A \exp(-t_D/\tau)$. The corresponding rate constant for desorption η is defined to be τ^{-1}.

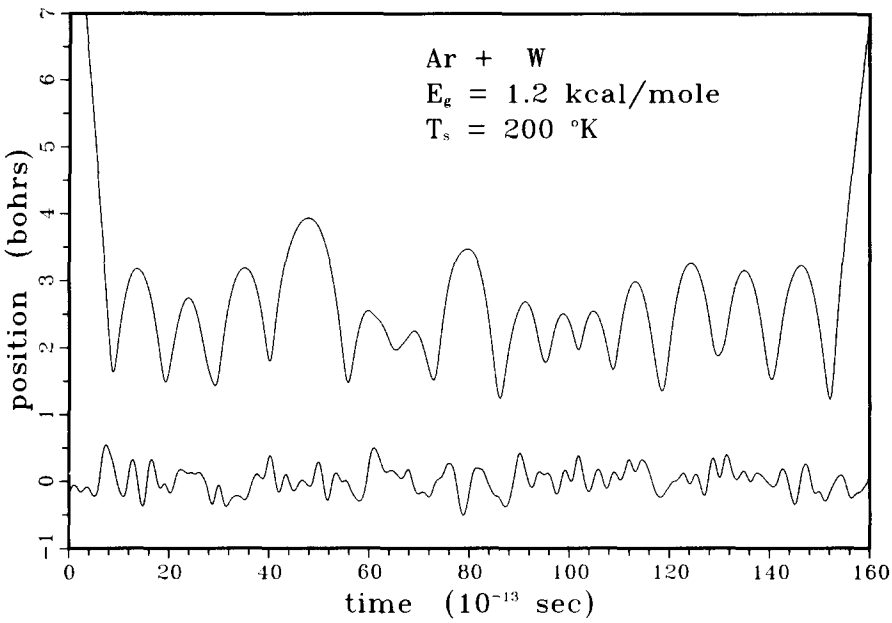

FIG. 9. An example of a trapped trajectory.

We define a mean residence time of an atom on the surface (including contributions from direct trajectories) to be

$$t_R = \int t_D P(t_D)\, dt_D \quad . \tag{28}$$

Now that we have defined a mean residence time and a desorption rate, we can use detailed balance to obtain a sticking probability, κ. In steady state, the number of atoms sticking to the surface has to be balanced by the number of atoms leaving. If I is the flux of incoming particles, then It_R is the mean density per unit area of particles on the surface. The rate of particles desorbing from the surface, $\eta I t_R$, must then equal the rate of particles sticking, $I\kappa$; i.e.,

$$\kappa = \eta t_R \quad . \tag{29}$$

We will take this as our definition of sticking probability. Our nonzero temperature studies were carried out for an argon atom colliding with the generalized Langevin oscillator (Case I) and with the Case II Brownian oscillator. Case II, again, is the classical definition of the Brownian approximation. For Ar, the critical trapping energy determined in the 0 °K study is about 0.9 kcal/mole for both of these models. We have measured the lifetimes and sticking probabilities as previously defined in each of these systems for monoenergetic beams of energy 1.2 kcal/mole and for surface temperatures of 200 °K and 300 °K. The results are given in Table III. A histogram of the function $P(t)$ for one of these cases is given in Fig. 7. The effect of incident energy on both of these models is the same, serving only to change the fraction of direct versus delayed trajectories. The lifetime τ of the atoms which stick on the surface longer than a few vibrational periods is not affected by the incident energy. The lifetime decreases with increasing surface temperature, as expected.

We have also monitored the final energy distribution of the gas particles as a function of time delay. This distribution peaks at high energy for particles with small time delay, and at larger times levels off to an energy characteristic of the surface temperature.

V. DISCUSSION

The object of this work was to investigate the potential value of the classical stochastic trajectory approach for simulating real gas–surface dynamical processes. We have described techniques for constructing generalized friction kernels and fluctuating forces which accurately represent the effects of the solid. We have presented convenient procedures for incorporating these terms into the numerical solution of the trajectories describing particle motion.

We have performed classical stochastic trajectory and quantum mechanical distorted-wave calculations on the same model, using identical input, and have shown that the results are in remarkably good agreement. We have demonstrated that it is feasible to apply the method to studies of adsorption and desorption processes. The effects of the solid, which are manifested via the generalized friction and fluctuating forces, are seen to

TABLE III. Mean residence times, rates of desorption, and sticking probabilities.

T_s(°K)	E_g(kcal/mole)	$\eta(10^{12}$ sec$^{-1})$	$\tau_R(10^{-12}$ sec)	κ
A. Generalized Langevin oscillator (Case I)				
200	1.2	0.11	4.1	0.45
200	2.4	0.12	1.9	0.23
300	1.2	0.18	2.9	0.52
300	2.4	0.19	1.6	0.30
B. Brownian oscillator (Case II)				
200	1.2	0.11	3.3	0.36
200	2.4	0.11	1.5	0.17
300	1.2	0.21	3.0	0.63
300	2.4	0.18	1.6	0.29

be very important and qualitatively understandable.

In summary, the stochastic trajectory approach appears to be a tractable and potentially accurate way to investigate the dynamics of a wide variety of gas–surface interaction phenomena. As with the closely related gas-phase classical trajectory approach, its most serious drawback lies not with its accuracy or difficulty of implementation, but rather with the current lack of realistic gas–surface interaction potentials required as input to the method.

APPENDIX: GENERATION OF THE RANDOM FORCE AND DAMPING INTEGRAL

We wish to generate a Gaussian random variable $R(t)$ which exhibits an autocorrelation function of the form

$$\langle R(0)R(t)\rangle = \frac{kT}{m}\Gamma_0 e^{-(1/2)\gamma t}\left[\cos(\omega_1 t) + \tfrac{1}{2}\gamma\omega_1^{-1}\sin(\omega_1 t)\right]$$

$$= mkT\Lambda(t) \quad . \tag{A1}$$

Since this function has memory of previous times, it is not Markovian. However, as discussed by Wang and Uhlenbeck,[15] it can be thought of as the "projection" of a Markov process in a higher (2D) space. Because of this, we can generate $R(t)$ from knowledge of it and its time derivative $\dot{R}(t)$ at any single previous time, using a conditional probability function defined as follows: $P(R, \dot{R}, t\,|R_0, \dot{R}_0, 0)$ is the conditional probability that if the variables $R(t)$ and $\dot{R}(t)$ have the values R_0 and $\dot{R}_0$ at time 0, they will have the values R and $\dot{R}$ at time t. The conditional probability function for a Brownian oscillator satisfying Eq. (A1) is given by Wang and Uhlenbeck:

$$P(R, \dot{R}, t\,|R_0, \dot{R}_0, 0) = (2\pi\sigma_x\sigma_y)^{-1}(1-\rho^2)^{-1/2}\exp\left[-\frac{1}{2(1-\rho^2)}\left(\frac{(R-\bar{R})^2}{\sigma_x^2} - \frac{2\rho(R-\bar{R})(\dot{R}-\bar{\dot{R}})}{\sigma_x\sigma_y} + \frac{(\dot{R}-\bar{\dot{R}})^2}{\sigma_y^2}\right)\right] , \tag{A2}$$

with means and variances

$$\bar{R} = \omega_1^{-1}\dot{R}_0 e^{-(1/2)\gamma t}\sin(\omega_1 t) + R_0 e^{-(1/2)\gamma t}\left[\cos(\omega_1 t) + \tfrac{1}{2}\gamma\omega_1^{-1}\sin(\omega_1 t)\right] , \tag{A3}$$

$$\bar{\dot{R}} = \dot{R}_0 e^{-(1/2)\gamma t}\left[\cos(\omega_1 t) - \tfrac{1}{2}\gamma\omega_1^{-1}\sin(\omega_1 t)\right] - \omega_0^2\omega_1^{-1}R_0 e^{-(1/2)\gamma t}\sin(\omega_1 t) , \tag{A4}$$

$$\sigma_y^2 = \langle(\dot{R}-\bar{\dot{R}})^2\rangle = \omega_0^2\Gamma_0\left\{1 - \omega_1^{-2}e^{-\gamma t}\left[\omega_1^2 + \tfrac{1}{2}\gamma^2\sin^2(\omega_1 t) - \gamma\omega_1\sin(\omega_1 t)\cos(\omega_1 t)\right]\right\} , \tag{A5}$$

$$\sigma_x^2 = \langle(R-\bar{R})^2\rangle = \Gamma_0\left\{1 - \omega_1^{-2}e^{-\gamma t}\left[\omega_1^2 + \tfrac{1}{2}\gamma^2\sin^2(\omega_1 t) + \gamma\omega_1\sin(\omega_1 t)\cos(\omega_1 t)\right]\right\} , \tag{A6}$$

$$\rho^2 = \langle(R-\bar{R})(\dot{R}-\bar{\dot{R}})\rangle = \Gamma_0\gamma\omega_0^2\omega_1^{-2}e^{-\gamma t}\sin^2(\omega_1 t) , \tag{A7}$$

$$\omega_0^2 = \omega_1^2 + \gamma^2/4 \quad . \tag{A8}$$

It is more convenient in the numerical generation of this process to express the two-dimensional Gaussian probability distribution as a product of two, one-dimensional Gaussian distributions. This is easily done by defining reduced variables

$$x = \frac{R-\bar{R}}{\sigma_x} , \tag{A9}$$

and

$$y = \frac{\dot{R}-\bar{\dot{R}}}{\sigma_y} , \tag{A10}$$

and completing the squares in the exponent of Eq. (A2). This procedure gives

$$P(R\dot{R}t\,|R_0\dot{R}_0 0) = (\sigma_x\sigma_y)^{-1}(1-\rho^2)^{-1/2} \times P(x)\,P[(y-\rho x)(1-\rho^2)^{-1/2}] , \tag{A11}$$

where

$$P(x) = (2\pi)^{-1/2}\exp(-\tfrac{1}{2}x^2). \tag{A12}$$

Equations (A2)–(A12) allow us to compute $R(t)$ and $\dot{R}(t)$ at any point along the trajectory from their values at the previous point by generating two independent Gaussian variables x and $(y-\rho x)(1-\rho^2)^{-1/2}$. We accomplish this computationally by employing a rational approximation to the inverse error function. The resulting $R(t)$ displays the autocorrelation function Eq. (A1) exactly, a fact which we have verified numerically. Note that with a predictor–corrector type integrator such as the one used here, a new value of the random force must be generated only at the predictor step and retained for the corrector.

In addition to generating the random force, we must evaluate the generalized friction integral which enters into the GLE, Eq. (4). Since the random force and generalized friction are related through the fluctuation-dissipation theorem, Eq. (8), it is necessary that they be consistent in order that surface temperature be maintained correctly over time. If it were necessary to explicitly evaluate friction as a quadrature over past times, the numerical implementation of the GLE would become very cumbersome. Fortunately, the Brownian oscillator form which we have chosen for the damping kernel allows one to avoid this problem entirely.

$\Lambda(t)$ of Eq. (19) is a solution of the differential equation

$$\ddot{\Lambda}(t) + \omega_0^2\Lambda(t) + \gamma\dot{\Lambda}(t) = 0 , \tag{A13}$$

where ω_0 is defined in Eq. (A8). The friction integral we wish to evaluate at each step along the trajectory is

$$y(t) = \int_0^t \Lambda(t-t')\dot{x}(t')\,dt' . \tag{A14}$$

Differentiating Eq. (A14) twice, and using Eq. (A13), we obtain[14]

$$\dot{y}(t) = z(t) \quad , \tag{A15}$$

$$\dot{z}(t) = -\omega_0^2 y(t) - \gamma z(t) + \Lambda_0 \ddot{x}(t) + \gamma \Lambda_0 \dot{x}(t) \quad . \tag{A16}$$

Since $\ddot{x}$ and $\dot{x}$ are generated at each point along the trajectory the damping can be evaluated easily by including Eqs. (A15) and (A16) as two additional first-order differential equations to be integrated along with all of the Hamilton equations for the particle positions and momenta. Thus a generalized Langevin equation with random force and damping of the form employed here can be integrated numerically with only a modest increase in computation time over the ordinary set of Hamilton's equations involving the same number of particles. For all of the nonzero temperature calculations reported here, including the Brownian limit, we carried out careful numerical verifications that the correct surface temperature was maintained.

[1]R. M. Logan and R. E. Stickney, J. Chem. Phys. **44**, 195 (1966); R. M. Logan and J. C. Keck, J. Chem. Phys. **49**, 860 (1968).

[2]R. A. Oman, J. Chem. Phys. **48**, 2919 (1968); J. Lorenzen and L. M. Raff, J. Chem. Phys. **49**, 1165 (1968); J. D. McClure, J. Chem. Phys. **51**, 1687 (1969); **57**, 2810 (1972); **57**, 2823 (1972).

[3]F. O. Goodman and H. Wachman, in *Dynamic Aspects of Surface Physics*, edited by F. O. Goodman (Editrice Compositori, Bologna, 1974), p. 347–529.

[4]S. A. Adelman and J. D. Doll, J. Chem. Phys. **61**, 4242 (1974).

[5]S. A. Adelman and J. D. Doll, J. Chem. Phys. **64**, 2375 (1976).

[6]R. Kubo, Rep. Prog. Theor. Phys. **29**, 255 (1966).

[7]H. Mori, Prog. Theor. Phys. **33**, 423 (1965).

[8]J. D. Doll, L. E. Myers, and S. A. Adelman, J. Chem. Phys. **63**, 4908 (1975).

[9]S. A. Adelman, J. Chem. Phys. **64**, 124 (1976).

[10]S. A. Adelman and B. Garrison, J. Chem. Phys. **65**, 3751 (1976).

[11]J. D. Doll and D. R. Dion, J. Chem. Phys. 65, 3762 (1976).

[12]For a review of this approach and relevant references, see F. O. Goodman, Surf. Sci. **24**, 667 (1971).

[13]See, for example, D. L. Bunker, Methods Comput. Phys. 10, 287 (1971).

[14]A. A. Maradudin, E. W. Montroll, G. H. Weiss, and I. P. Ipatova, *Theory of Lattice Dynamics in the Harmonic Approximation* (Academic, New York, 1971), 2nd ed.

[15]M. C. Wang and G. E. Uhlenbeck, Rev. Mod. Phys. 17, 323 (1945)

[16]This functional form for the friction kernel has also been suggested by Adelman and Garrison (Ref. 10). However, the procedure they propose for generating the random force is inconsistent with this form. Their random force is also limited by its finite recurrence time. The method we describe in the Appendix is precisely consistent with the friction kernel, Eq. (19). Furthermore, it in principle has an infinite recurrence time and in practice is limited only by the recurrence length of whatever random number generator is employed.

[17]J. M. Jackson and N. F. Mott, Proc. R. Soc. London Ser. A 137, 703 (1932).

[18]Doll and Dion (Ref. 11) have carried out similar calculations using a random force and damping kernel that exhibit a simple exponential time dependence, corresponding to a Lorentzian density of states peaked at $\omega = 0$. This can be considered intermediate between our form, Eq. (19), and the Brownian limit and provides further useful information about this point.